Strong magnetic exchange coupling in Ln2 metallocenes attained by the trans-coordination of a tetrazinyl radical ligand

Journal:	*Inorganic Chemistry Frontiers*
Manuscript ID	QI-RES-02-2023-000290.R1
Article Type:	Research Article
Date Submitted by the Author:	06-Jun-2023
Complete List of Authors:	Mavragani, Niki ; University of Ottawa Kitos, Alexandros ; University of Ottawa Hrubý, Jakub; National High Magnetic Field Laboratory - Florida State University Hill, Stephen; National High Magnetic Field Laboratory - Florida State University Mansikkamäki, Akseli; University of Oulu, NMR Research Unit Moilanen, Jani; University of Jyväskylä Murugesu, Muralee; University of Ottawa

ARTICLE

Strong magnetic exchange coupling in Ln_2 metallocenes attained by the *trans*-coordination of a tetrazinyl radical ligand†

Received 00th January 20xx,
Accepted 00th January 20xx

DOI: 10.1039/x0xx00000x

Niki Mavragani,[a] Alexandros A. Kitos,[a] Jakub Hrubý,[b] Stephen Hill,[b,c] Akseli Mansikkamäki,[d] Jani O. Moilanen,[e] and Muralee Murugesu*[a]

A combination of high-performing lanthanide metallocenes and tetrazine-based radical ligands leads to a new series of radical-bridged dinuclear lanthanide metallocenes; $[(Cp^*_2Ln^{III})_2(bpytz^{\bullet-})][BPh_4]$ (where Ln = Gd (**1**), Tb (**2**), Dy (**3**) and Y (**4**); Cp* = pentamethylcyclopentadienyl; bpytz =3,6-bis(3,5-dimethyl-pyrazolyl)-1,2,4,5-tetrazine). The formation of the radical species is achieved *via* a controlled, stepwise synthesis and verified in all complexes by X-ray crystallography and SQUID magnetometry, as well as EPR spectroscopy of **4**. Through the judicious choice of the Cp* ancillary ligands and by taking advantage of the steric effects imposed by their bulkiness, we were able to promote the *trans* coordination mode of the $bpytz^{\bullet-}$ radical anion that enables stronger magnetic exchange coupling compared to the *cis* fashion. This yields a $J_{Gd\text{-}rad}$ = -14.0 cm^{-1} in **1**, which is the strongest exchange coupling observed in organic monoanionic radical-bridged lanthanide metallocene systems. The strong Ln-rad exchange coupling was further confirmed by high-frequency EPR (HF-EPR) spectroscopy and broken symmetry (BS) density functional theory (DFT) calculations. This combined with the highly anisotropic nature of Tb^{III} and Dy^{III} ions in **2** and **3**, respectively, leads to strong SMM behavior and slow relaxation of the magnetization at zero fields.

Introduction

Single-molecule magnets (SMMs) exhibit magnet-like behaviour of magnetic remanence and hysteresis at the molecular level; thus, each molecule acts as a single-domain magnetic particle with bistability.[1,2] In recent years, mononuclear late lanthanide molecules (e.g., Tb^{III}, Dy^{III}, Er^{III}) with high anisotropy have been prominent examples of high-performing SMMs.[3–8] Namely, cyclopentadienyl-based molecular systems such as $[Cp^*DyCp^{iPr5}]^+$ (Cp* = pentamethylcyclopentadienyl; Cp^{iPr5} = pentaisopropylcyclopentadienyl) have shown that blocking of the magnetization above the temperature of liquid nitrogen can be reached through careful molecular design.[9] However, mononuclear SMMs are limited by the number of unpaired electrons and single-ion anisotropy as they only contain a single Ln^{III} ion. Thus, polynuclear systems are the way forward for attaining even higher performing SMMs.[10,11]

As simple as this approach might seem, the addition of more Ln ions into a system does not guarantee enhanced magnetic performance. Several attempts have been made over the years to create polynuclear Ln-based SMMs,[12–17] but enhancing and controlling their magnetic properties remains challenging. This stems from the shielded nature of *4f* orbitals which prevents inducing magnetic coupling between the Ln^{III} ions. A “radical” approach to overcome this challenge, is the introduction of paramagnetic linkers. Strong magnetic coupling between the metal centers and the radical species can give rise to a high angular momentum ground state, leading to blocking of the magnetization and slow magnetic relaxation.

A decade ago, a unique example of a paramagnetic linker that bridged two Ln centers highlighted the importance of magnetic coupling to SMM behaviour.[18] Consequently, research has focused on exploiting radical ligands[19–21] that can unlock the path towards attaining polynuclear lanthanide complexes that act as a single magnetic entity rather than a collection of magnetically uncoupled Ln^{III} ions in a molecular unit. Many organic radicals such as nitrozyl,[22–26] semiquinonoids[27–29] and verdazyl[30] have promoted magnetic coupling between Ln^{III} ions. However, most of them pale in comparison to the $N_2^{3\bullet-}$. This is because the strength of the magnetic coupling is of the essence; if the exchange Ln-rad coupling is weaker than the anisotropy of the individual Ln ions, there will be little to no improvement in the magnetic performance. Therefore, to design high-performing SMMs one needs a highly anisotropic system with appreciably strong magnetic coupling.

Amongst these organic radicals, tetrazine-based ligands stand out as they offer a clear synthetic advantage over the $N_2^{3\bullet-}$

---

[a] Department of Chemistry and Biomolecular Sciences, University of Ottawa, Ontario K1N 6N5, Canada.
[b] National High Magnetic Field Laboratory, Florida State University, Tallahassee, Florida 32310, United States.
[c] Department of Physics, Florida State University, Tallahassee, Florida 32306, United States.
[d] NMR Research Unit, University of Oulu, P.O. Box 300, 90014 Oulu, Finland.
[e] Department of Chemistry, Nanoscience Centre, University of Jyväskylä, P.O. Box 35, FI-40014, Finland

† Electronic Supplementary Information (ESI) available: Synthetic procedures, single-crystal X-ray diffraction data, additional magnetic, EPR and computational data. CCDC numbers 2158048, 2158049, 2158050 and 2158051. For ESI and crystallographic data in CIF or other electronic format see DOI: 10.1039/x0xx00000x

which leaves little room for modification. Although challenging, the design and synthesis of tetrazine-based ligands can lead to tetrazines with different substituents at the 3- and 6-positions of the ring.[31] In addition, the diffuse nature of the spin orbitals of the tetrazinyl radical ring is ideally suited to penetrate the shielded 4*f* orbitals, promoting strong magnetic coupling. Furthermore, the formation of the radical species is favored by the very low-lying π* LUMO of the ring, which can easily undergo one e^- reduction.[32] Recently, our group showcased the first examples of dinuclear $[(Cp^*_2Ln)_2(tz^{\bullet-})(THF)_2](BPh_4)$ (Ln = Gd, Tb or Dy; THF = tetrahydrofuran), ("$\mathbf{Ln_2}$")[33] and tetranuclear $[(Cp^*_2Ln)_4(tz^{\bullet-})_4]\cdot3(C_6H_6)$ (Ln = Gd or Dy), ("$\mathbf{Ln_4}$")[34] complexes containing lanthanide metallocene units bridged by the 1,2,4,5-tetrazine (tz) radical ligand. In both cases, the strong magnetic coupling between the Ln centers and the radicals led to the formation of a "giant-spin" model with slow relaxation of the magnetization at zero-field (for the "$\mathbf{Tb_2}$", "$\mathbf{Dy_2}$" and "$\mathbf{Dy_4}$" analogues) and granted the "$\mathbf{Dy_4}$" SMM a coercive field of ~30 kOe.

Inspired by this, we sought to investigate the well-explored 3,6-bis(3,5-dimethyl-pyrazolyl)-1,2,4,5-tetrazine (bpytz) ligand.[35] This linker has previously been shown to promote strong magnetic coupling with 3*d*[36] and 4*f* metals.[37,38] With regards to the latter, we once probed the incorporation of both the neutral bpytz in a Dy dimer $[Dy^{III}_2(\mu\text{-bpytz})(THMD)_6]$[37] as well as the radical $bpytz^{\bullet-}$ anion in a tetranuclear $[Dy_4(\mu_3\text{-}OH)_4(bpytz^{\bullet-})_2(TFA)_2(DBM)_4]$ cluster (where THMD 2,2,6,6-tetramethyl-3,5-heptanedionate; TFA = trifluoroacetate; DBM = dibenzoylmethanide).[38] In both cases, the magnetic properties of these complexes were moderate. In the case of the neutral bpytz, the complex exhibits SMM behavior under a small static applied field and Raman processes dominate the relaxation of the magnetization.[37] On the other hand, the reduction of the bpytz ligand in the Dy_4 cubane led to slightly better magnetic performance revealing a small U_{eff} = 21.9 cm^{-1} in the absence of a static magnetic field.[38] These differences in the magnetic properties of the aforementioned complexes clearly show the importance of the paramagnetic species in the bridging bpytz ligand and highlight its potential as a useful platform for the design of new high-performing SMMs. However, the effect of the binding mode of the tetrazine (*cis vs. trans*) on the magnetic coupling strength is yet to be demonstrated.

Therefore, through the judicious choice of the bpytz ligand we target to investigate the *trans* coordination mode and its overall effect on the magnetic properties. By taking advantage of the steric effects imposed by the bulkiness of the Cp* ancillary ligands, we can effectively target a novel series of dinuclear Ln-based metallocenes in which the metal centers are bridged through the *trans* coordination mode of the tetrazine radical ($bpytz^{\bullet-}$) (Scheme 1). Additional benefit of the employment of pentamethylcyclopentadienyl ligands (Cp*) instead of carboxylate or β-diketones is the enhancement of the magnetic performance of such complexes due to the well-known ability of the Cp* to afford a strong axial crystal field for oblate Ln^{III} ions, particularly in single ion systems.[8,9] We successfully isolated, through a stepwise synthetic approach, four dinuclear complexes with the general formula, $[(Cp^*_2Ln^{III})_2(bpytz^{\bullet-})](BPh_4)$ (where Ln = Gd (**1**), Tb(**2**), Dy (**3**) and Y (**4**); Cp* = pentamethylcyclopentadienyl). The formation of the radical was verified by both EPR and SQUID magnetometry measurements. Fitting of the magnetic data reveals the strongest exchange couplings mediated by an organic monoanionic radical observed in Ln metallocenes to this date for **1** ($J_{Gd\text{-}rad}$ = -14.0 cm^{-1}). This was further confirmed by broken symmetry (BS) density functional theory (DFT) calculations, as well as high-frequency EPR (HF-EPR) spectroscopy of **1**. Accordingly, the SMM behavior of **1**, **2** and **3** was examined, where slow relaxation of the magnetization was observed for **2** and **3** both in the absence and presence of a static dc field. Overall, these remarkable magnetic properties demonstrate the importance of the different coordination mode (*cis vs. trans*) of the radical bridging ligand and its effect on the magnetic coupling with the metal ions.

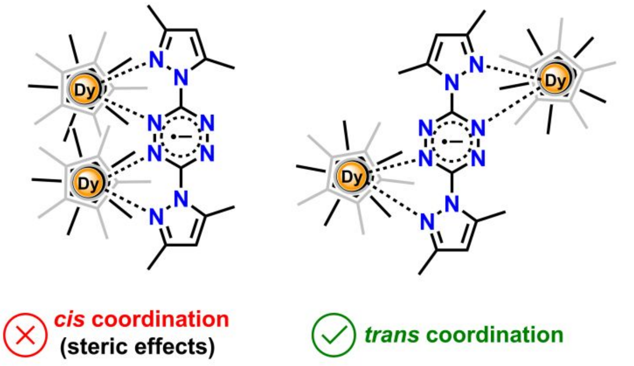

Scheme 1. Exploitation of the steric effects imposed by the bulkiness of the pentamethylcyclopentadienyl co-ligands to promote the *trans* coordination mode of the $bpytz^{\bullet-}$ ligand.

Results and discussion

Synthetic procedure and structural description

The syntheses of **1**-**4** start with the reduction of the tetrazine ligand. An equimolar mixture of the bpytz ligand and cobaltocene (Cp_2Co) was prepared in THF (Fig. 1, top). This was added to a solution of two equivalents of $[Cp^*_2Ln^{III}][(\mu\text{-}Ph_2)BPh_2]$ (where Ln = Gd, Tb, Dy or Y). The resulting dark purple solution was stirred for two hours, filtered, and placed in an Et_2O bath. After two days, dark purple crystals of **1**-**4** were obtained in ~60 % yields (based on the ligand). It is noteworthy that the same reaction can be performed in toluene following the same step-by-step approach. However, due to the poor solubility of these complexes in toluene, the yield and quality of the resulting crystals significantly decreased.

All four complexes crystallize in the orthorhombic $Pna2_1$ space group and possess the same structural topology, which was also confirmed by infrared spectroscopy (Fig. S1). Given this, dysprosium congener **3** was chosen as the representative example to describe the salient structural features of these complexes. The molecular structure of **3** is shown in Fig. 1 (bottom) and Fig. S2. X-ray data and selected distances and

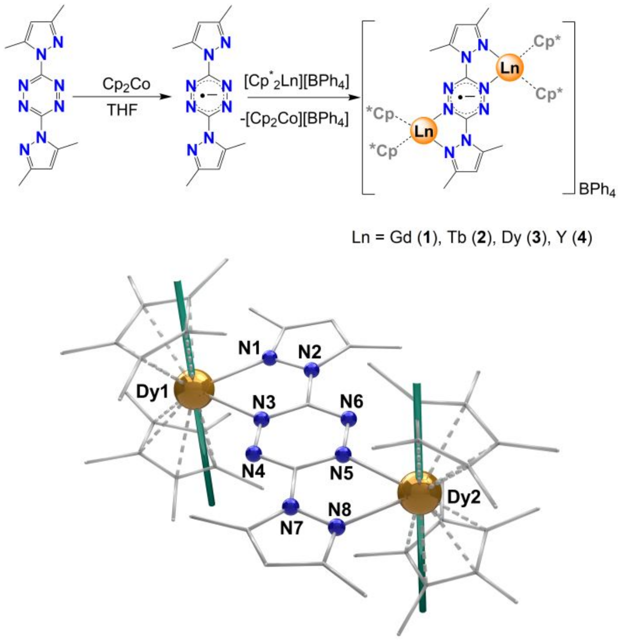

Figure 1. (Top) Synthetic scheme for the radical-bridged dinuclear complexes **1-4**. (Bottom) Molecular structure of **3**. For clarity, partial labelling and omission of the BPh_4^- moiety and H-atoms was employed. The solid teal lines represent the orientation of the *ab initio* calculated principal magnetic axes of the ground Kramers doublet. Color code: C: light grey; N: blue; Dy: orange.

angles are given in Tables S1 and S2. The dinuclear metal complex **3** consists of two independent (Dy1 and Dy2) Dy^{III} ions bridged by one $bpytz^{\bullet-}$ ligand, in a *trans* coordination mode, four η^5-Cp* co-ligands (two on each metal site) and one tetraphenylborate counter ion. Evidence for the one-electron reduction of the bpytz ligand is first provided by the elongation of the N=N bonds within the tetrazine moiety, which are beyond 1.36 Å, suggests the formation of the radical anion.[32] Here, the average N=N bonds within the tetrazine ring of bpytz correspond to 1.388(16), 1.387(15), 1.389(17) and 1.410(10) Å, for **1**, **2**, **3** and **4**, respectively, a clear indication of the reduced nature of the bpytz ligand.[37,38] The paramagnetic nature of the reduced $bpytz^{\bullet-}$ of the radical anion was further confirmed by EPR, SQUID magnetometry and computational studies of **4** (*vide infra*). The average Dy-C_{Cp*} distance and Cp^*_{cent}-Dy-Cp^*_{cent} (cent = centroid of the Cp* ring) angle was found to be 2.365(5) Å and 141.52(24)°, respectively, with an overall slight increase in the axiality compared to the previously reported $tz^{\bullet-}$-bridged "$\mathbf{Dy_2}$" (Dy-Cp^*_{cent}: 2.395(5) Å and Cp^*_{cent}-Dy-Cp^*_{cent}: 136.58(2)°)[33] and "$\mathbf{Dy_4}$" complexes (Dy-Cp^*_{cent}: 2.379(2) Å and Cp^*_{cent}-Dy-Cp^*_{cent}: 137.86(4)°).[34] The Dy-$N_{tetrazine}$ and Dy-$N_{pyrazole}$ bond distances (2.419(12) and 2.423(13) Å for Dy1, 2.402(12) and 2.395(13) Å for Dy2, respectively) are slightly shorter compared to previously reported Ln-$bpytz^{\bullet-}$ complexes (2.455(6)-2.569(4) Å)[37,38] likely due to the weaker coordination and the steric effects of the Cp* co-ligands compared to the stronger coordination of the less bulky carboxylate or *β*-diketones derivatives (Fig. 2). Due to the different coordination mode of the ligand (*cis* vs. *trans*) the torsion angle of Dy1-$N_{tetrazine}$-$N_{tetrazine}$-Dy2 can vary and it was found to be equal to -148.0(35)° in **3**, significantly higher compared to the previously reported[38] Ln_4-$bpytz^{\bullet-}$ complexes (11.3(8)°). Such variation in bond lengths is anticipated to yield significant differences in magnetic properties, specifically in the strength of the magnetic exchange interactions (*vide infra*). On the supramolecular level, the absence of strong hydrogen bonding donors or acceptors in both the main residue and solvent area of **3**, leads mostly to weak H···H and C···H interactions. The packing arrangement displays short intermolecular Dy···Dy interactions of 8.908(8) Å, while the Dy···Dy intramolecular distance is 7.548(9) Å (Fig. S3).

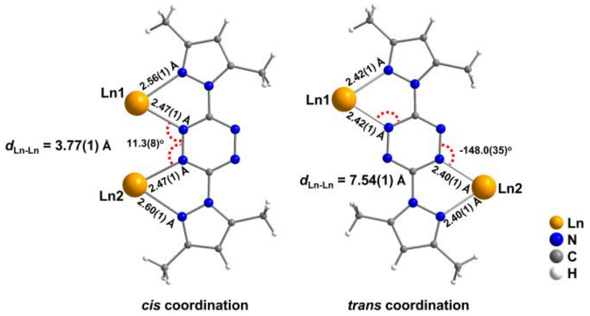

Figure 2. Structural comparison of the previously reported $[Dy_4(\mu_3\text{-}OH)_4(bpytz^{\bullet-})_2(TFA)_2(DBM)_4]$ complex[38] (*cis* coordination mode of $bpytz^{\bullet-}$) with the $[(Cp^*_2Ln^{III})_2(bpytz^{\bullet-})][BPh_4]$ reported herein (*trans* coordination mode of $bpytz^{\bullet-}$). The *trans* coordination fashion is found to promote stronger magnetic exchange coupling ($J_{Gd\text{-}rad}$ = -14 cm^{-1}; this work) compared to the *cis* coordination mode ($J_{Gd\text{-}rad}$ = -2.83 cm^{-1}; calculated, this work; $J_{Dy\text{-}rad}$ = -7.63 cm^{-1}; *vide infra*).[39]

Magnetic measurements, EPR and computational studies

To elucidate the magnetic behavior of **1**-**4**, direct current (dc) and alternating current (ac) magnetic susceptibility studies were conducted. The dc magnetic susceptibilities of **1**, **2** and **3** were measured between 300 and 1.8 K at 1000 Oe (Fig. 3A). The χT products, at room temperature, are 16.09, 23.93 and 28.69 cm^3 K mol^{-1} for **1**, **2** and **3**, respectively. These values are consistent with the theoretical values of 16.13, 24.01 and 28.71 cm^3 K mol^{-1}, for **1**, **2** and **3**, respectively for two Ln^{III} ions (Gd: S = 7/2, $^8S_{7/2}$, g = 2, C = 7.88 cm^3 K mol^{-1}; Tb: S = 3, L = 3, $^7F_6$, g = 3/2, C =11.82 cm^3 K mol^{-1}; Dy: S = 5/2, L = 5, $^6H_{15/2}$, g = 4/3, C = 14.17 cm^3 K mol^{-1}) and one radical anion (S = ½, C = 0.37 cm^3 K mol^{-1}). The χT products for **1**, **2** and **3** increase steadily with the decrease in temperature, reaching a maximum of 24.68 cm^3 K mol^{-1} at 8 K for **1**, 37.63 cm^3 K mol^{-1} at 26 K for **2** and a value of 46.65 cm^3 K mol^{-1} at 14 K for **3**. This behavior can be ascribed to the spin alignment of the Ln^{III} ions which is caused by the strong antiferromagnetic interaction between the $bpytz^{\bullet-}$ ligand and the metal centers, as has been previously seen in other radical-bridged Ln metallocenes.[33,34,40,41] For **1**, below 8 K, the χT product decreases with the decrease in temperature, reaching a value of 23.24 cm^3 K mol^{-1} at 1.8 K. For **2**, below 26 K, the χT decreases slightly with the temperature drop, ending at a shallow minimum of 36.44 cm^3 K mol^{-1}. Then an abrupt increase is observed upon further lowering of the temperature, until it reaches a maximum of 36.71 cm^3 K mol^{-1} at 4 K. Similarly, to this, a sudden increase of the χT product is observed below 13 K for **3**, reaching a maximum of 49.01 cm^3 K mol^{-1} at 5.5 K. This sudden rise is probably attributed to intermolecular

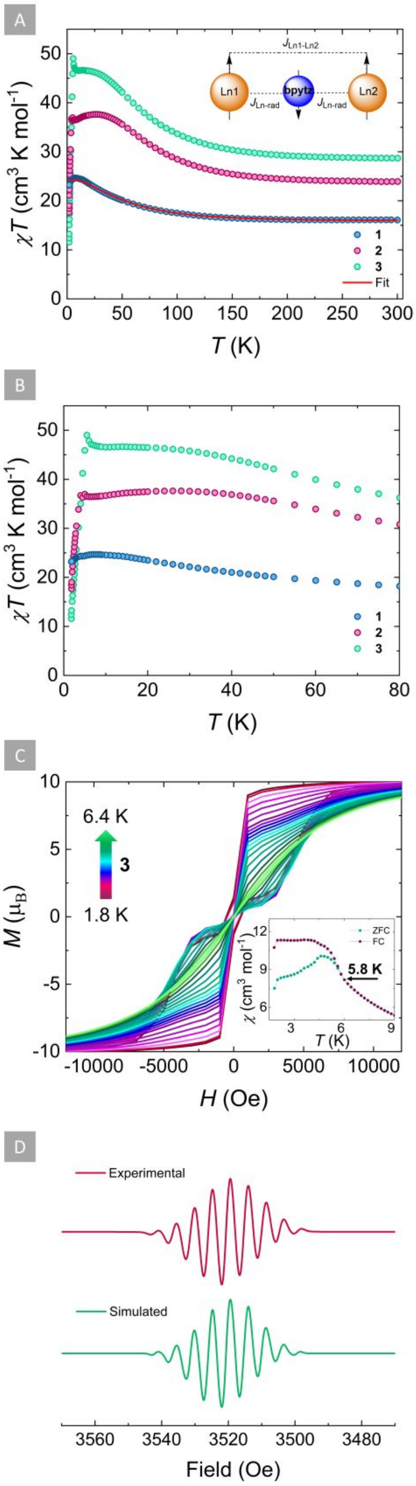

Figure 3. (A) Variable temperature χT plots of **1** (blue circles), **2** (purple circles) and **3** (teal circles) under an applied static field of 1000 Oe. The solid red line represents the fit as determined from applying the -2*J* formalism. Inset: Simplified illustration of the *J*-model, which was used to fit the data highlighting the antiparallel spin alignment between the Ln^{III} ions and the $\text{bpytz}^{\bullet-}$ ligand. (B) Zoomed-in area between 1.8 and 80 K, highlighting the behavior of the χT product at the low temperature region. (C) Hysteresis sweep from 1.8 to 6.4 K for **3**, in the field range of 70 kOe to -70 kOe, with an average sweep rate of 31 Oe/s. Inset: Zero-field-cooled and field-cooled (ZFC/FC) curves for **3** under an applied static field of 1000 Oe. Data were collected at an average sweep rate of 0.14 K/min. The black arrow indicates ZFC and FC susceptibilities bifurcate at 5.8 K for **3**. (D) Experimental (magenta) and simulated (teal) EPR spectra of **4** in THF (at room temperature) (g = 2.0014; SW = 10 mT; LW = 0.2 mT; a_{N1} = 0.596 mT; a_{N2} = 0.468 mT).

interactions between the Ln^{III} ions[42] which are enhanced by the short intermolecular $\text{Ln}^{\text{III}}\cdots\text{Ln}^{\text{III}}$ distances (Fig. S3). Finally, for both complexes (**2** and **3**), upon further lowering of the temperature, the χT decreases rapidly with decreasing temperature to reach a value of 17.64 cm^3 K mol^{-1} for **2** and 11.56 cm^3 K mol^{-1} for **3** at 1.8 K (Fig. 3B). This rapid plummeting of the χT value at low temperatures is indicative of magnetic blocking, as observed for other lanthanide systems.[7,43]

To verify the presence of magnetic blocking, zero-field-cooled/field-cooled (ZFC/FC) magnetic susceptibility measurements were performed for **2** and **3**. The divergence of the two data sets at 4.4 K for **2** (Fig. S5; inset) and 5.8 K for **3** (Fig. 3C; inset) supports the strong pinning of the magnetic moment below this temperature region. Moreover, the field dependence of the magnetization (up to 70 kOe) at various temperatures (1.9-7 K) was measured, for both complexes, revealing *s*-shaped curves between 1.9-3 K for **2** and 1.9-5 K for **3** (Fig. S6), further supporting the blocking of the magnetization at these temperatures. Consequently, magnetic hysteresis measurements were undertaken in varying fields (from -70 kOe to 70 kOe), using an average sweep rate of 31 Oe/s. For **2**, butterfly-shaped hysteresis loops were observed in the temperature range of 1.8 to 5.4 K, above which they are no longer open (Fig. S5). For **3**, between 1.8 and 2 K, at H_{dc} = 0 Oe, waist-restricted hysteresis loops are observed (Fig. 3C and S7). Above 2.4 K, a crossing of the magnetization is observed, which is indicative of quantum tunneling of the magnetization (QTM). At higher temperatures, the hysteresis loops are open until 6.4 K, above which they are no longer open, further confirming the magnetic blocking occurring around this temperature range.

As aforementioned, the radical nature of the tetrazine unit was verified not only through crystallographic means but also by EPR spectroscopy, SQUID magnetometry measurements and computational studies for the Y-based congener, **4**. Compared to other diamagnetic rare earths, such as La(III), Y(III) is often preferred for the synthesis of diamagnetic analogues of SMMs[42,44–46] as it offers a clear advantage. Y(III) possesses a stable isotope (^{89}Y) with a natural abundance of 100%, a nuclear spin of ½ and its ionic radius is similar to that of Gd(III), Tb(III) and Dy(III).[47] These enable detail information of the electronic structures when subjecting the corresponding Y(III) complexes to invaluable characterization methods such as EPR spectroscopy, as well as to computational studies.[48] The EPR spectrum of **4**, revealed the characteristic nine-line pattern attributed to the tetrazine ring of the $\text{bpytz}^{\bullet-}$ (i.e., simulated using a model based on the hyperfine coupling of four ^{14}N nuclei with two slightly different isotropic hyperfine coupling constants (IHCCs) for the coordinated and non-coordinated ^{14}N atoms; a_{N1} = 0.596 mT and a_{N2} = 0.468 mT; Fig. 3D). The isotropic hyperfine coupling constants (a_{N}) obtained from the simulation, were in good agreement with the calculated ones and showed that the coupling to ^{89}Y nuclei is weaker (Table S16). The inclusion of ^{89}Y nuclei into the simulation did not improve the simulated EPR spectrum. In addition, the dc magnetic susceptibility of **4** was measured between 300 and 1.8 K at 1000 Oe (Fig. S8). The room temperature χT product has a value of 0.36 cm^3 K mol^{-1} which is in good agreement with the theoretical value for one radical species (S = ½, C = 0.37 cm^3 K mol^{-1}). Upon lowering of the temperature, the χT product remains relatively stable until 5 K. Below this temperature, it decreases rapidly, reaching a minimum of 0.24 cm^3 K mol^{-1} at 1.8 K. This sudden downturn of the χT product at low temperatures suggests the presence of antiferromagnetic intermolecular interactions between the radical bpytz$^{\bullet-}$ moieties. These interactions were effectively accounted for in the fit of the χT plot (zJ = -0.37 cm^{-1}). The weak nature of these interactions is supported by the intermolecular rad···rad distances of 10.846(4) Å and 11.011(4) Å (Fig. S4).

As evident by the increase of the χT products with the decrease in temperature in **1**-**3**, the lanthanide ions are strongly and antiferromagnetically coupled to the radical bridging ligand. For **2** and **3**, this coupling can give rise to a high-angular momentum ground state for the overall molecule, which can enable the blocking of the magnetization. Therefore, it is critical to assess the strength of this magnetic coupling. In **1**, the isotropic nature of the 4f^7 electronic configuration of the Gd^{III} ions, allows for this quantification. Consequently, the χT *vs* T plot of **1** was fitted, using PHI software,[49] to the spin-only Hamiltonian: $\hat{H} = -2J_{\text{Gd-rad}}\hat{S}_{\text{rad}}(\hat{S}_{\text{Gd1}} + \hat{S}_{\text{Gd2}}) - 2J_{\text{Gd1-Gd2}}\hat{S}_{\text{Gd1}}\hat{S}_{\text{Gd2}}$, where $J_{\text{Gd-rad}}$ represents the Gd^{III}-radical exchange coupling, $J_{\text{Gd1-Gd2}}$ represents the intramolecular Gd^{III}-Gd^{III} exchange coupling and $\hat{S}_i$ are the spin operators for each paramagnetic center. The best fit resulted in $J_{\text{Gd-rad}}$ = -14.0 cm^{-1}, confirming the anticipated antiferromagnetic Gd^{III}-radical coupling. It is noteworthy that the large coupling constant value of the $J_{\text{Gd-rad}}$ = -14.0 cm^{-1} is likely due to the *trans* coordination mode of the radical bridging anion. In addition, due to the parallel alignment of the principal Ln^{III} ground state magnetic axes, the best fit also yielded $J_{\text{Gd1-Gd2}}$ = + 0.79 cm^{-1}, indicating the ferromagnetic coupling between the Ln^{III} centers. Attempts to use a negative $J_{\text{Gd1-Gd2}}$ or omit it from the fit, did not yield satisfactory fits. The field-dependent magnetization measurements further validate this for **1** at low temperatures. The magnetization plot (M *vs.* H, Fig. S6) shows field dependence, as it increases rapidly upon increasing the field, reaching a value of 12.92 $N\mu_B$ at 1.9 K and 70 kOe, which further supports a spin ground state of S_T = 13/2. For complexes **2** and **3**, the fit of the χT data employing similar methods is complicated given the intricate electronic structures of the individual Tb(III) and Dy(III) ions, respectively, which set a significant challenge when trying to accurately assign the absolute strength and/or sign of J.[40,43] However, since similar trends were observed in the temperature dependence of the χT data for **2** and **3**, it is reasonable to assume that the magnitudes of the antiferromagnetic Tb^{III}/Dy^{III}-bpytz$^{\bullet-}$ couplings are of comparable strength as proven in qualitatively manner (*vide infra*).

Furthermore, high-frequency EPR (HF-EPR) spectroscopy confirms the results of the magnetic fits - namely that **1** has a strongly coupled giant spin ground state (see ESI for further details; Fig. S9-S12). Notably, this is the highest exchange parameter reported for an organic monoanionic radical bridging Gd^{III} metallocene and it even surpasses the previously reported tz$^{\bullet-}$-bridged "**Gd$_4$**". This is only surpassed by $N_2^{3\bullet-}$ complexes, as shown in Table 1. We note that the recently reported example of a benzene dianionic radical ligand in [K(18-crown-6)(THF)$_2$]$_2$[Gd$_2$(BzN$_6$-Mes)] (BzN$_6$-Mes = 1,3,5-tris[2′,6′-(*N*-mesityl)dimethanamino-4′-*tert*-butylphenyl]benzene) was exempt from this comparison despite the impressive $J_{\text{Gd-rad}}$ = -43 cm^{-1}, due to its diradical nature (S = 1).[50]

To further support the experimental findings, we carried out the BS DFT calculations for four different cationic gadolinium model systems – **1Cp*$_{\text{trans}}$**, **1Cp*$_{\text{cis}}$**, **1Cp$_{\text{trans}}$**, and **1Cp$_{\text{cis}}$** – that were constructed from the crystal structure of **1** (Cp = cyclopentadienyl; Fig. 4 and SI). It is evident from the calculated data that the coordination of Gd^{III} ions in *cis* fashion leads to the strong twisting of bpytz$^{\bullet-}$ ligand, in particular, with the bulkier Cp* substituents (Fig. 4, S15, and Table S3).

Table 1. Comparison of the highest exchange parameters (-2J formalism) of radical-bridged Gd complexes.

	$J_{\text{Gd-rad}}$ (cm^{-1})	Ref.
$[\{((\text{SiMe}_3)_2\text{N})_2(\text{THF})\text{Gd}\}_2(\mu_3\text{-N}_2^{\bullet})\text{K}]$	-27.1	51
$[\text{K}(18\text{-crown-}6)]\{[(\text{Me}_3\text{Si})_2\text{N}]_2(\text{THF})\text{Gd}\}_2(\mu\text{-N}_2^{\bullet})$	-27.0	18
$[\text{K}(\text{crypt-}222)(\text{THF})][(\text{Cp}^{\text{Me4H}}{}_2\text{Gd}(\text{THF}))_2(\mu\text{-N}_2^{\bullet})]$	-20.0	52
$[(\text{Cp*}_2\text{Gd})_2(\text{bpytz}^{\bullet})](\text{BPh}_4)$	-14.0	This work
$[(\text{Cp*}_2\text{Gd})_4(\text{tz}^{\bullet})_4]\cdot3(\text{C}_6\text{H}_6)$	-12.0; -7.50	34
$[(\text{Cp*}_2\text{Gd})_2(\mu\text{-}5,5'\text{-F}_2\text{bpym}^{\bullet})](\text{BPh}_4)$	-11.1	53
$[\text{K}(\text{THF})_6][(\text{Cp*}_2\text{Gd})_2(\mu\text{-ind}^{\bullet})]\cdot\text{THF}$	-11.0	54
$[(\text{Cp*}_2\text{Gd})_2(\mu\text{-bpym}^{\bullet})](\text{BPh}_4)$	-10.0	40
$[(\text{Cp*}_2\text{Gd})_2(\mu\text{-}5,5'\text{-(Me)}_2\text{bpym}^{\bullet})](\text{BPh}_4)$	-9.54	53
$[(\text{Cp*}_2\text{Gd})_2(\text{tz}^{\bullet})(\text{THF})_2](\text{BPh}_4)$	-7.22	33
$[(\text{Cp*}_2\text{Gd})_2(\mu\text{-tppz}^{\bullet})](\text{BPh}_4)$	-6.91	43
$[\text{K}(\text{crypt-}222)][(\text{Cp*}_2\text{Gd})_2(\mu\text{-tppz}^{\bullet})]$	-6.29	43
$[(\text{Cp*}_2\text{Gd})_3(\mu_3\text{-HAN}^{\bullet})]$	-5.00	41
$[(\text{Cp*}_2\text{Gd})_2(\mu\text{-}5,5'\text{-(OEt)}_2\text{bpym}^{\bullet})](\text{BPh}_4)$	-4.16	53
$[(\text{Cp*}_2\text{Gd})_2(\mu\text{-}5,5'\text{-(NMe}_2)_2\text{bpym}^{\bullet})](\text{BPh}_4)$	-2.66	53
$[\text{K}(\text{crypt-}222)][(\text{Cp*}_2\text{Gd})_2(\mu\text{-Bbim}^{\bullet})]$	-1.96	55

THF = tetrahydrofuran; Cp$^{\text{Me4H}}$ = tetramethylcyclopentadienyl; Cp* = pentamethylcyclopentadienyl; tz = 1,2,4,5-tetrazine; bpym = 2,2′-bipyrimidine; tppz = 2,3,5,6-tetra(2-pyridyl)pyrazine; ind = indigo; HAN = hexaazatrinaphthylene; Bbim = 2,2′-bisbenzimidazole. All radical ligands presented herein have a S =½.

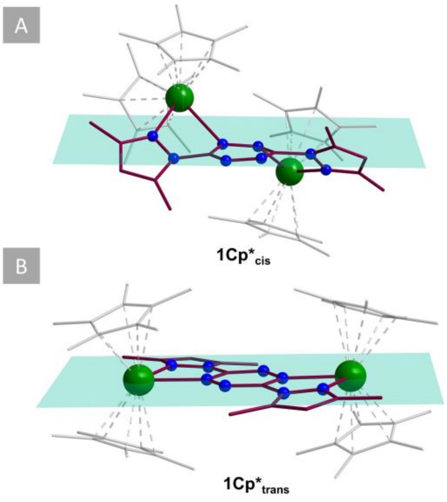

Figure 4. Gas-phase optimized geometries of **1Cp*$_{\text{cis}}$** (A) and **1Cp*$_{\text{trans}}$** (B) illustrating the strong twisting of the bpytz$^{\bullet-}$ in the *cis*-coordination mode *vs.* the *trans*-coordination mode where the ligand preserves its planarity. For clarity, H-atoms were omitted.

As a matter of fact, the steric hindrance in **1Cp***$_{\mathbf{cis}}$ is so strong that it is 110 kJ mol^{-1} higher in energy than **1Cp***$_{\mathbf{trans}}$ explaining why only the *trans* isomer of **1** is observed experimentally (Table S4). Between the less bulky Cp substituted isomers, namely **1Cp**$_{\mathbf{trans}}$, and **1Cp**$_{\mathbf{cis}}$, the energy difference is only 14 kJ mol^{-1} for the favor of the *trans* isomer. A more detailed inspection of the geometrical parameters reveals that the Gd-N$_{tetrazine}$, Gd-N$_{pyrazole}$ and Cp$_{cent}$-Gd distances are rather similar in all optimized model systems, but Cp$_{cent}$-Gd- Cp$_{cent}$ and Gd-N$_{tetrazine}$-N$_{tetrazine}$-Gd angles vary among the configurational isomers (Table S3). Among the studied compounds **1Cp***$_{\mathbf{trans}}$ has the most optimal geometrical parameters for the strong Gd-bpytz$^{\bullet-}$ exchange coupling because the calculated $J_{Gd\text{-}rad}$ are -11.07 cm^{-1}, -9.91 cm^{-1}, -2.83 cm^{-1}, and -5.65 cm^{-1} for **1Cp***$_{\mathbf{trans}}$, **1Cp**$_{\mathbf{trans}}$, **1Cp***$_{\mathbf{cis}}$, and **1Cp**$_{\mathbf{cis}}$, respectively (Table S5). The calculated results do not only support the (previous) experimental findings,[39] but they also show that the value of $J_{Gd\text{-}rad}$ is dictated by a delicate interplay between the steric hindrance of ancillary ligands and configurational isomerism in bpytz$^{\bullet-}$-based systems.

Given the large intrinsic magnetic anisotropy of Tb^{III} and Dy^{III} ions, it is anticipated that **2** and **3** will exhibit slow magnetic relaxation and thus act as SMMs. For comparison reasons, the slow relaxation of the magnetization in **1** was also explored. As such, ac magnetic susceptibility measurements were performed for complexes **1**-**3**, which indeed displayed frequency and temperature-dependent out-of-phase (χ'') susceptibility signals between 0.1-1488 Hz. For **1**, a peak of the χ'' susceptibility was observed only in the presence of a static dc field, which is expected for Gd(III)-based complexes.[56–58] Despite our best efforts, the frequency-dependent studies of the ac susceptibility, both with varying fields (Fig. S17, S18 and Table S17) and temperatures (Fig. S19, S20 and Table S18), revealed that the relaxation of the magnetization in **1** is dominated by QTM (Table S19; see ESI for further details). This is reasonable considering the very small ZFS parameters obtained from the HF EPR studies of **1** (D = +0.047 cm^{-1}; E = +0.009 cm^{-1}; E/D = 0.19). For **2**, a frequency-dependent signal was observed in the absence of a static dc field (H_{dc} = 0 Oe) between 9.2 and 1.8 K (Fig. 5A and S21). Both the in-phase (χ') and out-of-phase (χ'') parts of the susceptibility revealed a single frequency-dependent signal between 9.2 and 5.8 K, suggesting that the relaxation of the magnetization takes place through a thermally activated process in this temperature region. Upon further lowering of the temperature, the maxima of the χ'' signal start to overlap, suggesting that through-barrier relaxation mechanisms start to dominate. By using CCFit-2 software,[59] a generalized Debye model was used to fit both the χ' and χ'' (Fig. 5B), affording the relaxation times (τ) (Table S20). Insight into the magnetic relaxation dynamics of **2** in the absence of a static dc field, was gained by the analysis and fitting of the τ^{-1} *vs. T* plots (Fig. 6A), where a combination of QTM, Raman and Orbach mechanisms was used to accurately fit the relaxation times, using Eqn. (1):

$$\tau^{-1} = \tau_{QTM}^{-1} + CT^{n} + \tau_0^{-1}\exp(-U_{eff}/k_BT)\ (1)$$

where τ is the magnetic relaxation time, τ_{QTM} is the relaxation time for quantum tunnelling, C and n are parameters that describe the Raman relaxation, τ_0 is the attempt time and U_{eff} is the effective barrier to spin reversal. The best fit to Eqn. (1) afforded the following parameters: τ_{QTM} = 1.04 × 10^{-1} s, C = 0.49 s^{-1} K^{-n}, n = 2.09, τ_0 = 3.34 × 10^{-11} s and U_{eff} = 97.8 cm^{-1}.

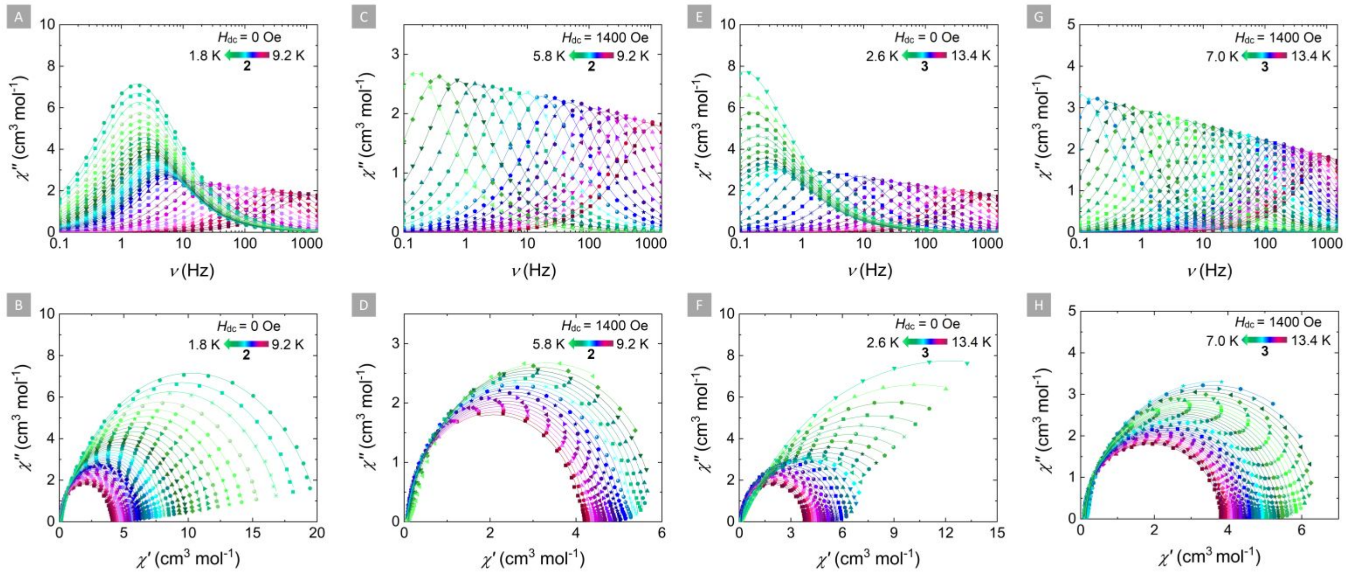

Figure 5. Frequency dependence of the out-of-phase magnetic susceptibility (χ'') for **2** (H_{dc} = 0 Oe; (A); H_{dc} = 1400 Oe; (C)) and **3** (H_{dc} = 0 Oe; (E); H_{dc} = 1400 Oe; (G)) and Cole-Cole plots for **2** (H_{dc} = 0 Oe; (B); H_{dc} = 1400 Oe; (D)) and **3** (H_{dc} = 0 Oe; (F); H_{dc} = 1400 Oe; (H)) at the respective temperature regions. Solid lines represent fits to the generalized Debye model. Fitting parameters for the generalized Debye fit of the ac susceptibilities for **2** are summarized in Table S20 (when H_{dc} = 0 Oe) and S25 (when H_{dc} = 1400 Oe) and for **3** in Table S21 (when H_{dc} = 0 Oe) and S26 (when H_{dc} = 1400 Oe).

Similarly to **2**, in the absence of a static magnetic field (H_{dc} = 0 Oe), a frequency-dependent signal was observed for **3** in the temperature range of 13.4 to 7.4 K (Fig. 5E and S22). At lower temperatures (7 to 2.6 K) this frequency-dependence is combined with a slight overlap of the χ'' signal, suggesting that through-barrier mechanisms contribute to the relaxation of the magnetization at lower temperatures. Fitting of both the χ' and χ'' to a generalized Debye model (Fig. 5F) affords the relaxation times (τ) (Table S21), which were fitted to a combination of QTM and Orbach mechanisms (Fig. 6B), using Eqn. (2):

$$\tau^{-1} = \tau_{QTM}^{-1} + \tau_0^{-1}\exp(-U_{eff}/k_BT) \quad (2)$$

A term accounting for Raman relaxation was also investigated without providing any physically meaningful parameters or improving the fit and was therefore removed. The best fit yielded $\tau_{QTM} = 6.88 \times 10^{-1}$ s, $\tau_0 = 1.00 \times 10^{-8}$ s and U_{eff} = 90.2 cm^{-1}. To find out whether the observed energy barriers originate from the spin-orbit states of a single Ln^{III} center or low-lying exchange states of **2** and **3**, we carried out the SA-CASSCF/SO-RASSI calculations for each individual Ln^{III} ion in **2** and **3**, as well as simulated their exchange-spectra at a qualitative level using the previously reported procedure[34] (see ESI for details). All calculations were performed with the Gaussian 16,[60] ORCA (5.0.3),[61] and the OpenMolcas (20.11)[62] quantum chemistry software. The first excited KDs of Dy^{III} ions are ~190 cm^{-1} higher in energy than their ground KDs (Tables S9–S10). Thus, for **3**, it is highly likely that the energy barrier for slow relaxation of the magnetization originates from the exchange state rather than from the individual Dy^{III} ions. Indeed, the energy of the first-excited exchange state is 78 cm^{-1} for **3** which is in reasonable agreement with the experimentally determined value of 97.8 cm^{-1} (Table S11). For **2**, the analysis is not as unbroken as for **3**, because, both the first excited pseudo doublets of the individual Tb^{III} ions (~115 cm^{-1}) and the first excited exchange state (65 cm^{-1}) are close to the experimental value of 90.2 cm^{-1} (Tables S7, S8 and S11). However, taking into account the strong exchange interaction observed for these complexes, it is more likely that the U_{eff} for **2** is also dictated by the exchange coupling.

Despite the contribution of QTM to the magnetic relaxation of these complexes, these U_{eff} are among the largest observed for tetrazine-based radical-bridged Ln^{III} complexes.[37,38,42,63] They surpass the previously reported U_{eff} for the tz$^{\bullet-}$-bridged "**Ln$_2$**" (49 cm^{-1} for the "**Tb$_2$**" and 25 cm^{-1} for the "**Dy$_2$**")[33] and are even comparable to the "**Dy$_4$**" (91 cm^{-1} and 80 cm^{-1}).[34] This can be rationalized by the slightly better axiality of the {Cp*$_2$Ln^{III}}$^+$ moieties in **2** and **3** (**3**: Cp*$_{cent}$-Dy-Cp*$_{cent}$: 141.52(24)°; "**Dy$_2$**": Cp*$_{cent}$-Dy-Cp*$_{cent}$: 136.58(2)°; "**Dy$_4$**": Cp*$_{cent}$-Dy-Cp*$_{cent}$: 137.86(4)°).

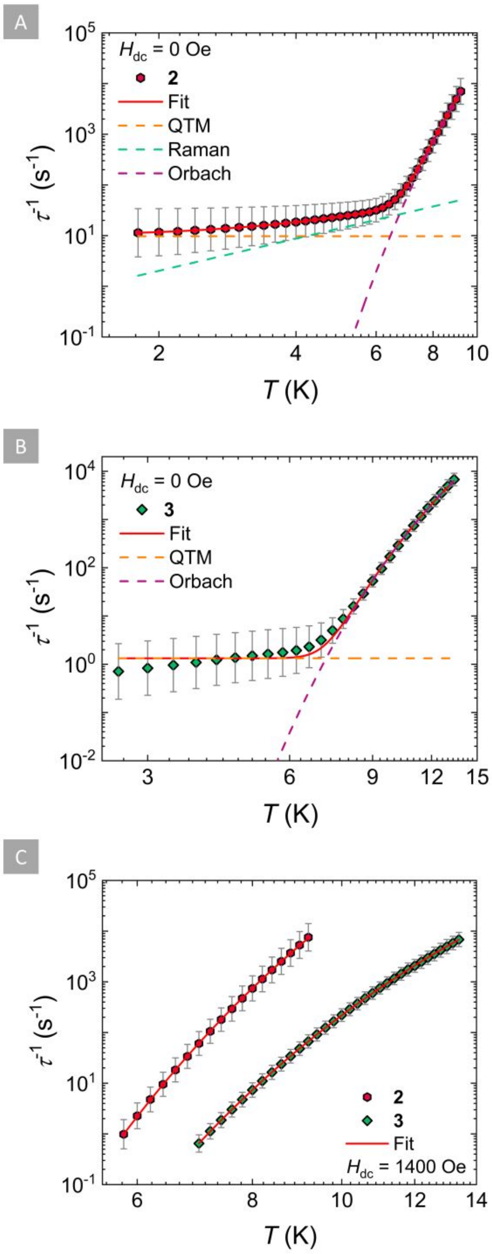

Figure 6. Temperature-dependence of the relaxation rates (τ^{-1}) for **2** (A) and **3** (B) when H_{dc} = 0 Oe and when H_{dc} = 1400 Oe (C) with the respective estimated standard deviations (gray bars). These estimated standard deviations of the relaxation times have been calculated from the α-parameters of the generalized Debye fits with the log-normal distribution.[59] The solid red lines represent the best-fit based on Eqn. (1) for (A), Eqn. (2) for (B) and Eqn. (3) for (C), while the dashed orange, teal and purple lines represent the individual components of the magnetic relaxation for QTM, Raman and Orbach processes, respectively.

The through-barrier relaxation of the magnetization in **3** can, in part, be attributed to the different coordination mode mediated by the $N_{pyrazole}$ on the Dy^{III} ions as well as to dissimilar effective charges of the coordinated atoms compared to "$\mathbf{Dy_4}$" that generate different crystal fields for **3** and $\mathbf{Dy_4}$ (see ESI). In other words, the coordination of the $bpytz^{\bullet-}$ at the equatorial positions of the Dy^{III} ions, through the 3,5-dimethyl-pyrazole substituents and the tetrazine ring, introduces QTM and competes with the axiality imposed by the Cp* groups, thus lowering the observed U_{eff}. This is probably further exacerbated by the close intermolecular $Ln^{III}\cdots Ln^{III}$ distances, which can lead to significant dipole-dipole interactions that are known to facilitate through-barrier relaxation of the magnetization.[64]

The effect of the applied static field on the magnetization dynamics of **2** and **3**, was examined to eliminate the presence of QTM. As such, ac measurements were undertaken at various static fields (0-5000 Oe) at a constant temperature of 6.5 K for **2** and 7.5 K for **3**, where a field-dependent signal of the χ'' was observed (Fig. S23 and S24, respectively). Fitting of the χ'' data *via* a generalized Debye model yielded the field-dependent τ for both complexes (Tables S22 and S23, respectively). For **2**, as evident by Fig. S25, an increase in the relaxation times with the increase of the applied static field is observed between 0 and 1400 Oe and above this field, the relaxation times start to decrease slightly. Comparatively to **2**, as seen in Fig. S26, the relaxation times for **3** show a similar increase with increasing applied static field up to 1400 Oe. However, above this field, the relaxation times become field-independent, indicating that QTM has been successfully suppressed at higher fields and that the relaxation of the magnetization is mediated exclusively *via* the thermally activated pathway. To further understand the relaxation dynamics taking place under the different applied static fields, the τ^{-1} *vs. H* plots for both **2** and **3** were fitted. For **2** a combination of QTM, Raman, Orbach and direct mechanisms was used in order to accurately fit the data. For **3** a satisfactory fit was achieved for a combination of QTM and Orbach (see ESI for further details). These trends are in agreement with those observed from the temperature-dependent studies of both complexes at H_{dc} = 0 Oe. Apart from the contribution of the direct mechanism in **2** (which is only present at higher applied dc fields), it is evident that the relaxation of the magnetization can be described by the same combination of processes; QTM, Raman and Orbach for **2**; QTM and Orbach for **3** (Table S24).

Following this, and since the presence of a static field can lead to effective suppression of QTM, the ac susceptibilities of both complexes were measured at 1400 Oe. For both complexes, the presence of a frequency-dependent peak of the χ'' susceptibility in the temperature range of 9.2 to 5.8 K for **2** (Fig. 5C, 5D, S27) and 13.4 to 7.0 K for **3** (Fig. 5G, 5H and S28), was observed. Fitting of the ac susceptibility data using a generalized Debye model yielded longer relaxation times (Table S25 for **2** and S26 for **3**). As expected, in both cases, the peaks of the susceptibility showed an exponential increase upon lowering of the temperature, indicative of a thermally activated relaxation process, i.e. Orbach mechanism. As such, the relaxation times were fitted, using Eqn. (3) (Fig. 6C):

$$\tau^{-1} = \tau_0^{-1}\exp(-U_{eff}/k_B T) \quad (3)$$

The best-fit parameters for **2** were $\tau_0 = 3.43 \times 10^{-11}$ s and U_{eff} = 97.2 cm^{-1}, showing, as expected, the suppression of QTM and Raman contributions. Similarly, for **3**, the best-fit parameters were $\tau_0 = 6.04 \times 10^{-9}$ s and U_{eff} = 94.1 cm^{-1}, showing that, as expected, upon suppression of the QTM the U_{eff} can be slightly enhanced. Accordingly, the Arrhenius plot for both complexes of the $\ln(\tau)$ *vs.* T^{-1} was constructed to verify these findings, where a linear trend was observed (Fig. S29). Best-fit parameters for the relaxation of the magnetization in the absence and presence of a static dc field for both complexes are summarized in Table S27.

Conclusions

Through a carefully designed strategy using a bulky metallocene building block and a redox-active ligand with two coordination pockets, a family of dinuclear Ln_2 complexes was successfully synthesized. In these complexes, the *trans* coordination mode of the bridging tetrazinyl radical ligand allowed us to probe the strength of the magnetic coupling which was significantly stronger compared to the *cis*-coordination fashion.[37–39] The highly localized spin density on the core of the tetrazinyl radical ring, in combination with the *trans* coordination mode of the $bpytz^{\bullet-}$ ligand dictated by the bulkiness of the Cp* ligands, leads to the strongest magnetic coupling reported for an organic monoanionic radical-bridged Ln metallocene ($J_{Gd\text{-}rad}$ = -14.0 cm^{-1}). Upon combination of this radical ligand with highly anisotropic $\{Cp^*_2Tb^{III}\}^+$ and $\{Cp^*_2Dy^{III}\}^+$ moieties in **2** and **3**, respectively, blocking of the magnetization and slow relaxation of the magnetization were observed with U_{eff} = 97.8 cm^{-1} for **2** and 90.2 cm^{-1} for **3**. These are the highest U_{eff} reported among the family of tetrazine-based radical-bridged Ln complexes. Interestingly, **1** also exhibited ac susceptibility signal in the presence of an applied dc field. However, the relaxation of the magnetization was dominated by QTM. These findings highlight the importance of the magnetic exchange coupling in 4*f*-based SMMs and prove that tetrazines are among the most prosperous organic radical ligands to promote such strong magnetic interactions. That said, different substituents on the 3- and 6-positions of the tetrazine ring can promote slow magnetic relaxation and enhance the magnetic communication between Ln ions. Through engineered design, tetrazines provide a new reliable platform for synthesizing high-performing SMMs.

Data availability

The data supporting the findings of this study are available within the article and in the ESI.†

Author Contributions

The manuscript was written through contributions of all authors.

Conflicts of interest

There are no conflicts to declare.

Acknowledgements

N. M., A. A. K. and M. M. thank the University of Ottawa, the Canada Foundation for Innovation (CFI) and the Natural Sciences and Engineering Research Council of Canada (NSERC) for the financial support of this work. N. M. acknowledges the University of Ottawa and the Stavros Niarchos Foundation for financial support through scholarships. J.H. and S. H. acknowledge support from the US Department of Energy, Basic Energy Sciences (DE-SC00012738). Work performed at the National High Magnetic Field Laboratory is supported by the US National Science Foundation (DMR-1644779) and the State of Florida. A. M. acknowledges funding provided by the Academy of Finland (grant no. 332294) and the University of Oulu (Kvantum Institute). J. O. M. acknowledges the Academy of Finland (projects 315829 and 345484) for the financial support, and the CSC-IT Centre for Science in Finland, the Finnish Grid and Cloud Infrastructure (persistent identifier urn:nbn:fi:research-infras-2016072533) and Prof. H. M. Tuononen (University of Jyväskylä) for providing computational resources for the project.

Notes and references

1 D. N. Woodruff, R. E. P. Winpenny and R. A. Layfield, Lanthanide Single-Molecule Magnets, *Chem. Rev.*, 2013, **113**, 5110–5148.
2 A. Zabala-Lekuona, J. M. Seco and E. Colacio, Single-Molecule Magnets: From Mn12-ac to dysprosium metallocenes, a travel in time, *Coord. Chem. Rev.*, 2021, **441**, 213984.
3 L. R. Thomas-Hargreaves, D. Hunger, M. Kern, A. J. Wooles, J. van Slageren, N. F. Chilton and S. T. Liddle, Insights into D4h@metal-symmetry single-molecule magnetism: the case of a dysprosium-bis(boryloxide) complex, *Chem. Commun.*, 2021, **57**, 733–736.
4 J. P. Durrant, B. M. Day, J. Tang, A. Mansikkamäki and R. A. Layfield, Dominance of Cyclobutadienyl Over Cyclopentadienyl in the Crystal Field Splitting in Dysprosium Single-Molecule Magnets, *Angew. Chem. Int. Ed.*, 2022, **61**, e202200525.
5 B. Ali, X.-L. Li, F. Gendron, B. L. Guennic and J. Tang, A new class of DyIII-SIMs associated with a guanidine-based ligand, *Dalton Trans.*, 2021, **50**, 5146–5153.
6 T. G. Ashebr, L. La Droitte, X.-L. Li, C. Zhao, J. Wu, Q. Zhou, O. Cador, B. Le Guennic and J. Tang, Edaravone-Based Mononuclear Dysprosium(III) Single-Molecule Magnets, *Cryst. Growth Des.*, 2022, **22**, 5063–5070.
7 K. L. M. Harriman, J. L. Brosmer, L. Ungur, P. L. Diaconescu and M. Murugesu, Pursuit of Record Breaking Energy Barriers: A Study of Magnetic Axiality in Diamide Ligated DyIII Single-Molecule Magnets, *J. Am. Chem. Soc.*, 2017, **139**, 1420–1423.
8 C. A. P. Goodwin, F. Ortu, D. Reta, N. F. Chilton and D. P. Mills, Molecular magnetic hysteresis at 60 kelvin in dysprosocenium, *Nature*, 2017, **548**, 439–442.
9 F.-S. Guo, B. M. Day, Y.-C. Chen, M.-L. Tong, A. Mansikkamäki and R. A. Layfield, Magnetic hysteresis up to 80 kelvin in a dysprosium metallocene single-molecule magnet, *Science*, 2018, **362**, 1400–1403.
10 C. A. Gould, K. R. McClain, D. Reta, J. G. C. Kragskow, D. A. Marchiori, E. Lachman, E.-S. Choi, J. G. Analytis, R. D. Britt, N. F. Chilton, B. G. Harvey and J. R. Long, Ultrahard magnetism from mixed-valence dilanthanide complexes with metal-metal bonding, *Science*, 2022, **375**, 198–202.
11 K. R. McClain, H. Kwon, K. Chakarawet, R. Nabi, J. G. C. Kragskow, N. F. Chilton, R. D. Britt, J. R. Long and B. G. Harvey, A Trinuclear Gadolinium Cluster with a Three-Center One-Electron Bond and an *S* = 11 Ground State, *J. Am. Chem. Soc.*, 2023, **145**, 8996–9002.
12 J.-T. Chen, H. Yan, T.-T. Wang, T.-D. Zhou and W.-B. Sun, Di- and Tetranuclear Dysprosium Single-Molecule Magnets Bridged by Unprecedentedly Disassembled Nitrogen-Enriched Tetrazine Derivatives, *Inorg. Chem.*, 2022, **61**, 19097–19105.
13 D. I. Alexandropoulos, S. Mukherjee, C. Papatriantafyllopoulou, C. P. Raptopoulou, V. Psycharis, V. Bekiari, G. Christou and T. C. Stamatatos, A New Family of Nonanuclear Lanthanide Clusters Displaying Magnetic and Optical Properties, *Inorg. Chem.*, 2011, **50**, 11276–11278.
14 M. A. Singh-Wilmot, R. A. Sinclair, M. Andrews, C. Rowland, C. L. Cahill and M. Murugesu, Nonanuclear lanthanide(III) nanoclusters: Structure, luminescence and magnetic properties, *Polyhedron*, 2013, **53**, 187–192.
15 S. K. Langley, N. F. Chilton, I. A. Gass, B. Moubaraki and K. S. Murray, Planar tetranuclear lanthanide clusters with the Dy4 analogue displaying slow magnetic relaxation, *Dalton Trans.*, 2011, **40**, 12656–12659.
16 S. K. Langley, B. Moubaraki, C. M. Forsyth, I. A. Gass and K. S. Murray, Structure and magnetism of new lanthanide 6-wheel compounds utilizing triethanolamine as a stabilizing ligand, *Dalton Trans.*, 2010, **39**, 1705–1708.
17 P.-H. Lin, T. J. Burchell, L. Ungur, L. F. Chibotaru, W. Wernsdorfer and M. Murugesu, A Polynuclear Lanthanide Single-Molecule Magnet with a Record Anisotropic Barrier, *Angew. Chem. Int. Ed.*, 2009, **48**, 9489–9492.
18 J. D. Rinehart, M. Fang, W. J. Evans and J. R. Long, Strong exchange and magnetic blocking in N23−-radical-bridged lanthanide complexes, *Nat. Chem.*, 2011, **3**, 538–542.
19 X. Ma, E. A. Suturina, S. De, P. Négrier, M. Rouzières, R. Clérac and P. Dechambenoit, A Redox-Active Bridging Ligand to Promote Spin Delocalization, High-Spin Complexes, and Magnetic Multi-Switchability, *Angew. Chem. Int. Ed.*, 2018, **57**, 7841–7845.
20 E. M. Fatila, M. Rouzières, M. C. Jennings, A. J. Lough, R. Clérac and K. E. Preuss, Fine-Tuning the Single-Molecule Magnet Properties of a [Dy(III)-Radical]2 Pair, *J. Am. Chem. Soc.*, 2013, **135**, 9596–9599.
21 M. B. Mills, C. A. Michalowicz, E. Song, A. C. Maahs, J. A. Newman, T. Cawte, J. M. Lovnicki, D. V. Soldatov and K. E. Preuss, A Supramolecular [π-radical]2 Unit Acts as a Ligand: Coordination of La and Ce by a Pancake-Bonded Pair, *Cryst. Growth Des.*, 2021, **21**, 5897–5903.
22 X.-L. Mei, R.-N. Liu, C. Wang, P.-P. Yang, L.-C. Li and D.-Z. Liao, Modulating spin dynamics of cyclic LnIII-radical complexes (LnIII = Tb, Dy) by using phenyltrifluoroacetylacetonate coligand, *Dalton Trans.*, 2012, **41**, 2904–2909.
23 F. Pointillart, K. Bernot, G. Poneti and R. Sessoli, Crystal Packing Effects on the Magnetic Slow Relaxation of Tb(III)-Nitronyl Nitroxide Radical Cyclic Dinuclear Clusters, *Inorg. Chem.*, 2012, **51**, 12218–12229.
24 S. Calancea, L. Carrella, T. Mocanu, V. Sadohin, M. Raduca, I. Gutu, J. C. da Rocha, M. G. F. Vaz, E. Rentschler and M. Andruh, Magnetic Molecular Rectangles Constructed from Functionalized Nitronyl-Nitroxide Ligands and Lanthanide(III) Ions, *Eur. J. Inorg. Chem.*, 2021, **2021**, 567–577.
25 M. Răducă, D. O. T. A. Martins, C. A. Spinu, M. Hillebrand, F. Tuna, G. Ionita, A. M. Mădălan, C. Lecourt, J.-P. Sutter and M. Andruh, A New Nitronyl-Nitroxide Ligand for Designing Binuclear LnIII Complexes: Syntheses, Crystal Structures,

Magnetic and EPR Studies, *Eur. J. Inorg. Chem.*, 2022, **2022**, e202200128.

26 M. Perfetti, A. Caneschi, T. S. Sukhikh and K. E. Vostrikova, Lanthanide Complexes with a Tripodal Nitroxyl Radical Showing Strong Magnetic Coupling, *Inorg. Chem.*, 2020, **59**, 16591–16598.

27 A. Caneschi, A. Dei, D. Gatteschi, L. Sorace and K. Vostrikova, Antiferromagnetic Coupling in a Gadolinium(III) Semiquinonato Complex, *Angew. Chem. Int. Ed.*, 2000, **39**, 246–248.

28 A. Dei, D. Gatteschi, C. A. Massa, L. A. Pardi, S. Poussereau and L. Sorace, Spontaneous symmetry breaking in the formation of a dinuclear gadolinium semiquinonato complex: Synthesis, high-field EPR studies, and magnetic properties, *Chem. - Eur. J.*, 2000, **6**, 4580–4586.

29 P. Zhang, M. Perfetti, M. Kern, P. P. Hallmen, L. Ungur, S. Lenz, M. R. Ringenberg, W. Frey, H. Stoll, G. Rauhut and J. van Slageren, Exchange coupling and single molecule magnetism in redox-active tetraoxolene-bridged dilanthanide complexes, *Chem. Sci.*, 2018, **9**, 1221–1230.

30 L. Norel, L.-M. Chamoreau, Y. Journaux, O. Oms, G. Chastanet and C. Train, Verdazyl-lanthanide(III) one dimensional compounds: synthesis, structure and magnetic properties, *Chem. Commun.*, 2009, 2381–2383.

31 O. Stetsiuk, A. Abhervé and N. Avarvari, 1,2,4,5-Tetrazine based ligands and complexes, *Dalton Trans.*, 2020, **49**, 5759–5777.

32 N. Mavragani, A. A. Kitos, J. L. Brusso and M. Murugesu, Enhancing Magnetic Communication between Metal Centres: The Role of s-Tetrazine Based Radicals as Ligands, *Chem. – Eur. J.*, 2021, **27**, 5091–5106.

33 N. Mavragani, A. A. Kitos, A. Mansikkamäki and M. Murugesu, New members of radical bridged Ln2 metallocene single-molecule magnets based on the unsubstituted 1,2,4,5-tetrazine ligand, *Inorg. Chem. Front.*, 2022, **10**, 259–266.

34 N. Mavragani, D. Errulat, D. A. Gálico, A. A. Kitos, A. Mansikkamäki and M. Murugesu, Radical-Bridged Ln4 Metallocene Complexes with Strong Magnetic Coupling and a Large Coercive Field, *Angew. Chem. Int. Ed.*, 2021, **60**, 24206–24213.

35 M. D. Coburn, G. A. Buntain, B. W. Harris, M. A. Hiskey, K.-Y. Lee and D. G. Ott, An improved synthesis of 3,6-diamino-1,2,4,5-tetrazine. II. From triaminoguanidine and 2,4-pentanedione, *J. Heterocycl. Chem.*, 1991, **28**, 2049–2050.

36 Z. Guo, Y.-F. Deng, Z. Pikramenou, K. R. Dunbar and Y.-Z. Zhang, Strong Coupling and Slow Relaxation of the Magnetization for an Air-Stable [Co4] Square with Both Tetrazine Radicals and Azido Bridges, *Inorg. Chem.*, 2021, **60**, 3651–3656.

37 M. A. Lemes, N. Mavragani, P. Richardson, Y. Zhang, B. Gabidullin, J. L. Brusso, J. O. Moilanen and M. Murugesu, Unprecedented intramolecular pancake bonding in a {Dy2} single-molecule magnet, *Inorg. Chem. Front.*, 2020, **7**, 2592–2601.

38 G. Brunet, M. Hamwi, M. A. Lemes, B. Gabidullin and M. Murugesu, A tunable lanthanide cubane platform incorporating air-stable radical ligands for enhanced magnetic communication, *Commun. Chem.*, 2018, **1**, 1–6.

39 V. Vieru, N. Iwahara, D. Komijani, S. Hill, W. Wernsdorfer and L. F. Chibotaru, Toward a Microscopic Understanding of the Magnetization Behavior of a Multimolecular Single Crystal of Radical-Bridged $[\mathrm{Dy}^{\mathrm{III}}{}_4]$ Cubane Units: A Joint Ab Initio, Micro-Superconducting Quantum Interference Device, and Electron Paramagnetic Resonance Study, *J. Phys. Chem. C*, 2018, **122**, 11128–11135.

40 S. Demir, J. M. Zadrozny, M. Nippe and J. R. Long, Exchange Coupling and Magnetic Blocking in Bipyrimidyl Radical-Bridged Dilanthanide Complexes, *J. Am. Chem. Soc.*, 2012, **134**, 18546–18549.

41 C. A. Gould, L. E. Darago, M. I. Gonzalez, S. Demir and J. R. Long, A Trinuclear Radical-Bridged Lanthanide Single-Molecule Magnet, *Angew. Chem. Int. Ed.*, 2017, **56**, 10103–10107.

42 B. S. Dolinar, D. I. Alexandropoulos, K. R. Vignesh, T. James and K. R. Dunbar, Lanthanide Triangles Supported by Radical Bridging Ligands, *J. Am. Chem. Soc.*, 2018, **140**, 908–911.

43 S. Demir, M. Nippe, M. I. Gonzalez and J. R. Long, Exchange coupling and magnetic blocking in dilanthanide complexes bridged by the multi-electron redox-active ligand 2,3,5,6-tetra(2-pyridyl)pyrazine, *Chem. Sci.*, 2014, **5**, 4701–4711.

44 G. Huang, X. Yi, J. Jung, O. Guillou, O. Cador, F. Pointillart, B. Le Guennic and K. Bernot, Optimization of Magnetic Relaxation and Isotopic Enrichment in Dimeric DyIII Single-Molecule Magnets, *Eur. J. Inorg. Chem.*, 2018, **2018**, 326–332.

45 Y.-C. Chen, J.-L. Liu, L. Ungur, J. Liu, Q.-W. Li, L.-F. Wang, Z.-P. Ni, L. F. Chibotaru, X.-M. Chen and M.-L. Tong, Symmetry-Supported Magnetic Blocking at 20 K in Pentagonal Bipyramidal Dy(III) Single-Ion Magnets, *J. Am. Chem. Soc.*, 2016, **138**, 2829–2837.

46 Y.-S. Ding, T. Han, Y.-Q. Zhai, D. Reta, N. F. Chilton, R. E. P. Winpenny and Y.-Z. Zheng, A Study of Magnetic Relaxation in Dysprosium(III) Single-Molecule Magnets, *Chem. – Eur. J.*, 2020, **26**, 5893–5902.

47 E. Castellanos and S. Demir, Linear, Electron-Rich, Homoleptic Rare Earth Metallocene and Its Redox Activity, *Inorg. Chem.*, 2023, **62**, 2095–2104.

48 S. E. Lorenz, B. M. Schmiege, D. S. Lee, J. W. Ziller and W. J. Evans, Synthesis and Reactivity of Bis(tetramethylcyclopentadienyl) Yttrium Metallocenes Including the Reduction of $\mathrm{Me_3SiN_3}$ to $[(\mathrm{Me_3Si})_2\mathrm{N}]^-$ with $[(\mathrm{C_5Me_4H})_2\mathrm{Y(THF)}]_2(\mu\text{-}\eta^2{:}\eta^2\text{-}\mathrm{N_2})$, *Inorg. Chem.*, 2010, **49**, 6655–6663.

49 N. F. Chilton, R. P. Anderson, L. D. Turner, A. Soncini and K. S. Murray, PHI: a powerful new program for the analysis of anisotropic monomeric and exchange-coupled polynuclear d- and f-block complexes, *J. Comput. Chem.*, 2013, **34**, 1164–1175.

50 C. A. Gould, J. Marbey, V. Vieru, D. A. Marchiori, R. David Britt, L. F. Chibotaru, S. Hill and J. R. Long, Isolation of a triplet benzene dianion, *Nat. Chem.*, 2021, **13**, 1001–1005.

51 K. R. Meihaus, J. F. Corbey, M. Fang, J. W. Ziller, J. R. Long and W. J. Evans, Influence of an Inner-Sphere K+ Ion on the Magnetic Behavior of N23– Radical-Bridged Dilanthanide Complexes Isolated Using an External Magnetic Field, *Inorg. Chem.*, 2014, **53**, 3099–3107.

52 S. Demir, M. I. Gonzalez, L. E. Darago, W. J. Evans and J. R. Long, Giant coercivity and high magnetic blocking temperatures for N 2 3− radical-bridged dilanthanide complexes upon ligand dissociation, *Nat. Commun.*, 2017, **8**, 2144.

53 C. A. Gould, E. Mu, V. Vieru, L. E. Darago, K. Chakarawet, M. I. Gonzalez, S. Demir and J. R. Long, Substituent Effects on Exchange Coupling and Magnetic Relaxation in 2,2′-Bipyrimidine Radical-Bridged Dilanthanide Complexes, *J. Am. Chem. Soc.*, 2020, **142**, 21197–21209.

54 F.-S. Guo and R. A. Layfield, Strong direct exchange coupling and single-molecule magnetism in indigo-bridged lanthanide dimers, *Chem. Commun.*, 2017, **53**, 3130–3133.

55 F. Benner, L. L. Droitte, O. Cador, B. L. Guennic and S. Demir, Magnetic hysteresis and large coercivity in bisbenzimidazole radical-bridged dilanthanide complexes, *Chem. Sci.*, 2023, **14**, 5577–5592.

56 Y. Masuda, S. Sakata, S. Kayahara, N. Irie, M. Kofu, Y. Kono, T. Sakakibara, Y. Horii and T. Kajiwara, Slow Magnetic Relaxation of Linear Trinuclear M(II)–Gd(III)–M(II) Complexes with D_3

Point Group Symmetry (M(II) = Zn(II) and Mg(II)), *J. Phys. Chem. C*, 2023, **127**, 3295–3306.

57 M. A. Dunstan, D. S. Brown, L. Sorace, R. A. Mole and C. Boskovic, Modulation of Slow Magnetic Relaxation in Gd(III)-Tetrahalosemiquinonate Complexes, *Chem. – Asian J.*, 2022, **17**, e202200325.

58 R. J. Holmberg, L. T. A. Ho, L. Ungur, I. Korobkov, L. F. Chibotaru and M. Murugesu, Observation of unusual slow-relaxation of the magnetisation in a Gd-EDTA chelate, *Dalton Trans.*, 2015, **44**, 20321–20325.

59 D. Reta and N. F. Chilton, Uncertainty estimates for magnetic relaxation times and magnetic relaxation parameters, *Phys. Chem. Chem. Phys.*, 2019, **21**, 23567–23575.

60 Gaussian 16, Revision C.01, M. J. Frisch, G. W. Trucks, H. B. Schlegel, G. E. Scuseria, M. A. Robb, J. R. Cheeseman, G. Scalmani, V. Barone, G. A. Petersson, H. Nakatsuji, X. Li, M. Caricato, A. V. Marenich, J. Bloino, B. G. Janesko, R. Gomperts, B. Mennucci, H. P. Hratchian, J. V. Ortiz, A. F. Izmaylov, J. L. Sonnenberg, D. Williams-Young, F. Ding, F. Lipparini, F. Egidi, J. Goings, B. Peng, A. Petrone, T. Henderson, D. Ranasinghe, V. G. Zakrzewski, J. Gao, N. Rega, G. Zheng, W. Liang, M. Hada, M. Ehara, K. Toyota, R. Fukuda, J. Hasegawa, M. Ishida, T. Nakajima, Y. Honda, O. Kitao, H. Nakai, T. Vreven, K. Throssell, J. A. Montgomery, Jr., J. E. Peralta, F. Ogliaro, M. J. Bearpark, J. J. Heyd, E. N. Brothers, K. N. Kudin, V. N. Staroverov, T. A. Keith, R. Kobayashi, J. Normand, K. Raghavachari, A. P. Rendell, J. C. Burant, S. S. Iyengar, J. Tomasi, M. Cossi, J. M. Millam, M. Klene, C. Adamo, R. Cammi, J. W. Ochterski, R. L. Martin, K. Morokuma, O. Farkas, J. B. Foresman, and D. J. Fox, Gaussian, Inc., Wallingford CT, 2016.

61 F. Neese, The ORCA program system, *WIREs Comput. Mol. Sci.*, 2012, **2**, 73–78.

62 I. Fdez Galván, M. Vacher, A. Alavi, C. Angeli, F. Aquilante, J. Autschbach, J. J. Bao, S. I. Bokarev, N. A. Bogdanov, R. K. Carlson, L. F. Chibotaru, J. Creutzberg, N. Dattani, M. G. Delcey, S. S. Dong, A. Dreuw, L. Freitag, L. M. Frutos, L. Gagliardi, F. Gendron, A. Giussani, L. González, G. Grell, M. Guo, C. E. Hoyer, M. Johansson, S. Keller, S. Knecht, G. Kovačević, E. Källman, G. Li Manni, M. Lundberg, Y. Ma, S. Mai, J. P. Malhado, P. Å. Malmqvist, P. Marquetand, S. A. Mewes, J. Norell, M. Olivucci, M. Oppel, Q. M. Phung, K. Pierloot, F. Plasser, M. Reiher, A. M. Sand, I. Schapiro, P. Sharma, C. J. Stein, L. K. Sørensen, D. G. Truhlar, M. Ugandi, L. Ungur, A. Valentini, S. Vancoillie, V. Veryazov, O. Weser, T. A. Wesołowski, P.-O. Widmark, S. Wouters, A. Zech, J. P. Zobel and R. Lindh, OpenMolcas: From Source Code to Insight, *J. Chem. Theory Comput.*, 2019, **15**, 5925–5964.

63 B. S. Dolinar, S. Gómez-Coca, D. I. Alexandropoulos and K. R. Dunbar, An air stable radical-bridged dysprosium single molecule magnet and its neutral counterpart: redox switching of magnetic relaxation dynamics, *Chem. Commun.*, 2017, **53**, 2283–2286.

64 F. Habib, P.-H. Lin, J. Long, I. Korobkov, W. Wernsdorfer and M. Murugesu, The Use of Magnetic Dilution To Elucidate the Slow Magnetic Relaxation Effects of a Dy_2 Single-Molecule Magnet, *J. Am. Chem. Soc.*, 2011, **133**, 8830–8833.